Dalton Transactions

ROYAL SOCIETY OF CHEMISTRY

PAPER

View Article Online
View Journal | View Issue

Check for updates

Cite this: *Dalton Trans.*, 2025, **54**, 5286

C–C and C–O bond formation reactivity of nickel complexes supported by the pyridinophane ^{Me}N3C ligand†

Joshua Ji-Nung Leung,‡ Dae Young Bae, ‡ Yusuff Moshood‡ and Liviu M. Mirica *

Received 17th January 2025,
Accepted 25th February 2025

DOI: 10.1039/d5dt00135h

rsc.li/dalton

The pyridinophane ligands ^{R}N3CX (X = H, Br) are well-established scaffolds that facilitate and stabilize nickel oxidative addition complexes to the proximal C(aryl)–X bond. In this study, we report the synthesis, detailed characterization, and reactivity of a series of Ni^{II} and Ni^{III} complexes supported by the ^{Me}N3CX ligand. Our findings demonstrate that Ni^{II} complexes can be oxidized to readily yield well-defined Ni^{III} species. Excitingly, the Ni-disolvento complexes exhibit catalytic trifluoroethoxylation to generate the C–O coupled product. In addition, the Ni^{III}-halide complex undergoes transmetallation with a Grignard reagent and subsequent C–C reductive elimination, while the β-hydride elimination side reaction is suppressed, outperforming its Ni^{II} analogue.

Introduction

High-valent organometallic nickel complexes have emerged as fascinating subjects of study due to their unique properties and potential applications in catalysis to forge new chemical bonds.[1–25] Among the various ligands employed to stabilize Ni^{III} centers, the tetradentate pyridinophane ligands, ^{R}N3CX, have supported high-valent Ni species with remarkable stability.[1] Understanding the stability of these complexes is crucial for reactivity study, and in particular, the role of substituent effects has been a topic of interest.[26–29] In this regard, replacing the *tert*-butyl (^{t}Bu) N-substituents with the less bulky neopentyl (Np) groups (yielding the ^{Np}N3C system) has been found to reduce stability and enhance the reactivity of the high valent nickel species compared to the ^{tBu}N3CX system.[28–30] Since the introduction of these systems, numerous metalloorganic systems based on this framework and incorporating first- and second-row transition metals such as Mn, Fe, Co, and Pd have been utilized to investigate their reactivity and catalytic processes.[31–40] Building upon the remarkable reactivity enhancement observed with Np N-substituents,[28,29] our current investigation explores the potential of the less bulky *N*-methyl analogues in stabilizing Ni^{III} intermediates.[31] In this case, the use of these methyl-substituted ligands aimed to elucidate the influence of steric effects on the reactivity of the nickel complexes. To generate the Ni^{III} centers, we employed both mild oxidants, allowing us to compare the reactivity and stability of the resulting complexes. The investigation aimed to shed light on the factors influencing the strength and significance of the agostic interactions between the Ni center and the *ipso* C(aryl)–H bond. Finally, in addition to stabilizing Ni^{III} intermediates and studying agostic interactions, we examined the oxidative addition of low-valent nickel systems into C–H bonds. This step allowed us to investigate the feasibility of C–H bond activation and its potential as a key step in various catalytic transformations.

Results and discussion

The Ni^{II} complex (^{Me}N3C)Ni^{II}Br (**1**) can be synthesized upon addition of Ni^{0}(COD)$_2$ to ^{Me}N3CBr following a modified literature procedure (Scheme 1).[31] The crystal structure of **1**, which has not been reported previously, reveals a trigonal bipyramidal geometry at the Ni center (Fig. 1), similar to its analog (^{tBu}N3C)Ni^{II}Br reported previously by our group.[26] The complex **1** can be oxidized by addition of one equivalent of FcPF$_6$ to yield the Ni^{III} complex [(^{Me}N3C)Ni^{III}Br(MeCN)]PF$_6$ (**3**). The solid-state structure of **3** could not be obtained, even upon substitution with different counterions (BArF$_{24}^{-}$, OTf^{-}, or BF$_4^{-}$), and complex identity was confirmed by ESI-MS and CHN analysis. Halide abstraction of the bromide from **3** by addition of one equivalent of TlPF$_6$, or abstraction and oxi-

Department of Chemistry, University of Illinois at Urbana-Champaign, 600 S. Mathews Avenue, Urbana, Illinois, 61801, USA. E-mail: mirica@illinois.edu

†Electronic supplementary information (ESI) available. CCDC 2390120 and 2390122–2390125. For ESI and crystallographic data in CIF or other electronic format see DOI: https://doi.org/10.1039/d5dt00135h

‡These authors contributed equally.

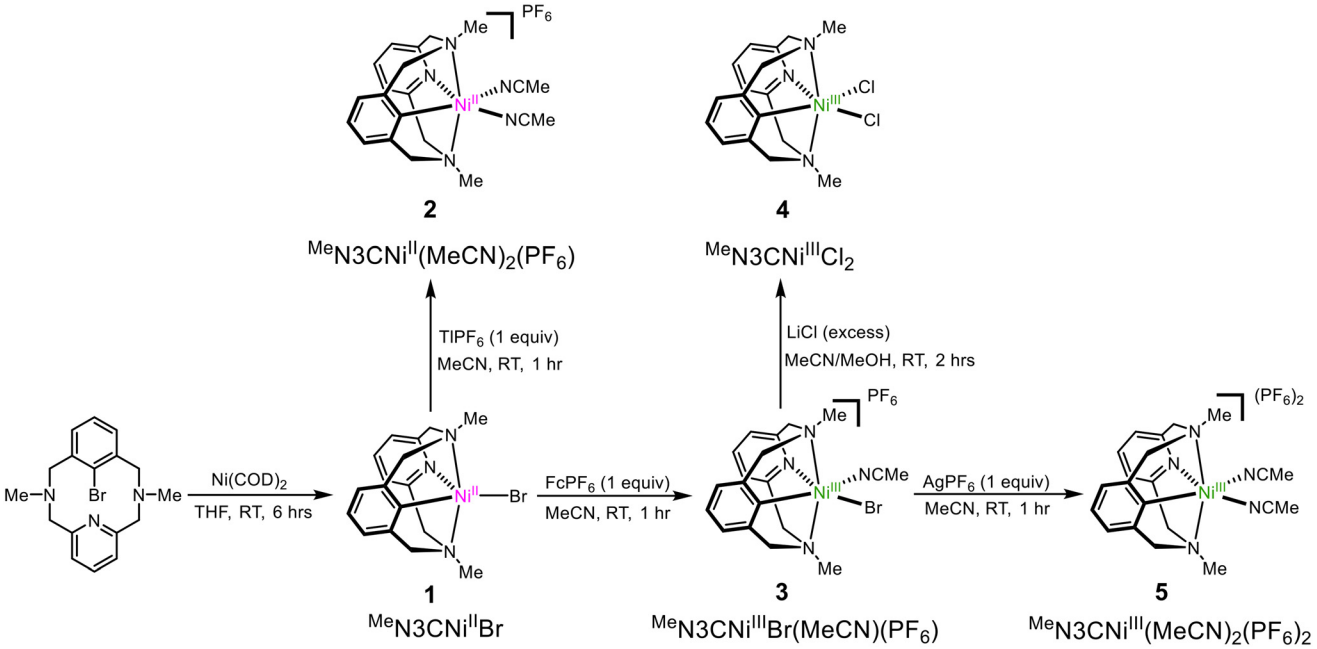

Scheme 1 Synthesis of (^{Me}N3C)Ni complexes.

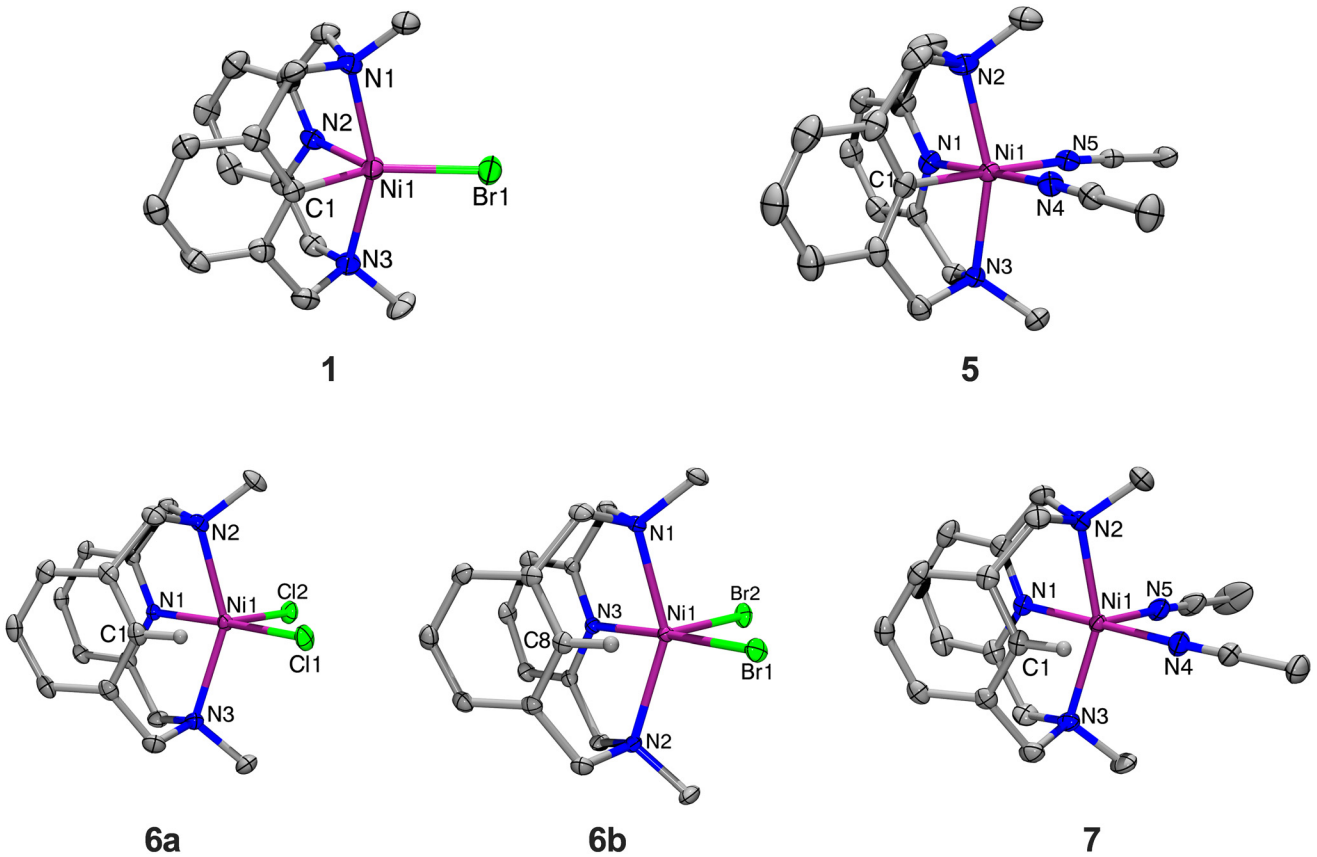

Fig. 1 ORTEPs (50% probability thermal ellipsoids) of complexes **1**, dication of **5**, **6a**, **6b**, and dication of **7**. For clarity, hydrogen atoms and counterions have been omitted. Selected bond distances (Å), **1**: Ni1–N1, 2.291(8); Ni1–N2, 1.981(7); Ni1–N3, 2.276(8); Ni1–C1, 1.954(9); Ni1–Br1, 2.372(2). **5**: Ni1–N1, 1.935(2); Ni1–N2, 2.152(2); Ni1–N3, 2.142(2); Ni1–N4, 1.983(2); Ni1–N5, 1.990(2); Ni1–C1, 1.921(2). **6a**: Ni1–N1, 1.993(2); Ni1–N2, 2.233(2); Ni1–N3, 2.242(2); Ni1–C1, 2.539(2); Ni–Cl1, 2.312(5); Ni–Cl2, 2.329(6). **6b**: Ni1–N1, 2.223(1); Ni1–N2, 2.255(1); Ni1–N3, 1.985(1); Ni1–C8, 2.482(2); Ni1–Br1, 2.455(4); Ni1–Br2, 2.478(4). **7**: Ni1–N1, 1.971(2); Ni1–N2, 2.179(2); Ni1–N3, 2.169(2); Ni1–N4, 2.023(2); Ni1–N5, 2.037(2); Ni1–C1, 2.412(2).

dation of **1** by addition of two equivalents of $AgPF_6$ yields the bis-solvento complex $[(^{Me}N3C)Ni^{III}(MeCN)_2](PF_6)_2$ (**5**). Both **3** and **5** are stable in air at RT. Evans method analysis of **3** and **5** returns magnetic moments of 1.89 and 1.80μ_B, indicating that both are paramagnetic with one unpaired electron, as expected for a d^7 Ni^{III} center. Structural characterization for **5** reveals an octahedral geometry as expected for d^7 ions, with the amine donors in the axial positions (Fig. 1). Their EPR characterizations (77 K, PrCN glass) show the presence of axial signals (Fig. 2) with g_{ave} values of 2.125 for **3**, along with superhyperfine coupling to the bromide (I = 3/2) is observed in the g_y direction, and a value of 2.109 for **5**, along with superhyperfine coupling to the two axial N donors (I = 1) in the g_z direction. Since the solid-state structure for complex **3** is elusive, excess LiCl was added for halide exchange to give rise to **4**.[31] The solid-state structure of **4** is also consistent with the previous observations for this system. However, a rhombic EPR signal was observed with g_{ave} 2.132, with no superhyperfine coupling to any halide. Taken together, the observed structural and EPR parameters for complexes **3**, **4**, and **5** strongly suggest the presence of a distorted octahedral Ni^{III} d^7 center with a d_z ground state.

Complexes $(^{Me}N3CH)Ni^{II}Cl_2$ (**6a**) and $(^{Me}N3CH)Ni^{II}Br_2$ (**6b**) were synthesized by stirring the corresponding NiX_2(dme) precursor with $^{Me}N3CH$ overnight, in 67% and 67% yields, respectively (Scheme 2). Halide abstraction *via* addition of 2 equivalents of $TlPF_6$ yielded the bis-solvento complex $(^{Me}N3CH)Ni^{II}(MeCN)_2(PF_6)_2$ (**7**) in 85% yield, and no C_{sp^2}–H activation was observed during the synthesis of **7**. Spin state analysis by Evans method of **6a**, **6b**, and **7** yielded magnetic moments of 3.16μ_B, 3.12μ_B, and 2.96μ_B, respectively, indicating that the three complexes are paramagnetic with two unpaired electrons. The solid-state structures show distorted square pyramidal geometries, with τ_5 values of 0.40, 0.42, and 0.41 respectively. Relatively short Ni–C lengths (2.539 Å, 2.482 Å, and 2.416 Å) and narrow Ni–H–C bond angles (94.0°, 96.3°, and 83.5°) are indicative of an agostic interaction in all three $(^{Me}N3CH)Ni^{II}$ complexes (Fig. 1). Notably, the Ni–H–C angle and Ni–C bond length increases as the σ-donor ancillary ligands are replaced by π-donor ligands. Even though these complexes are all prone to C–H activation, we postulate that the complex bearing σ-donor ancillary ligands are more prone to activation due to potentially stronger agostic interactions. It is known that C–H agostic interaction is an electronic effect which involves the donation of electron density associated with the C–H bond to a metal center.[41] Therefore, computational studies were employed in order to investigate the electronic structures. Density functional theory (DFT) calculations were performed at the B3LYP/def2-TZVPP level of theory, as

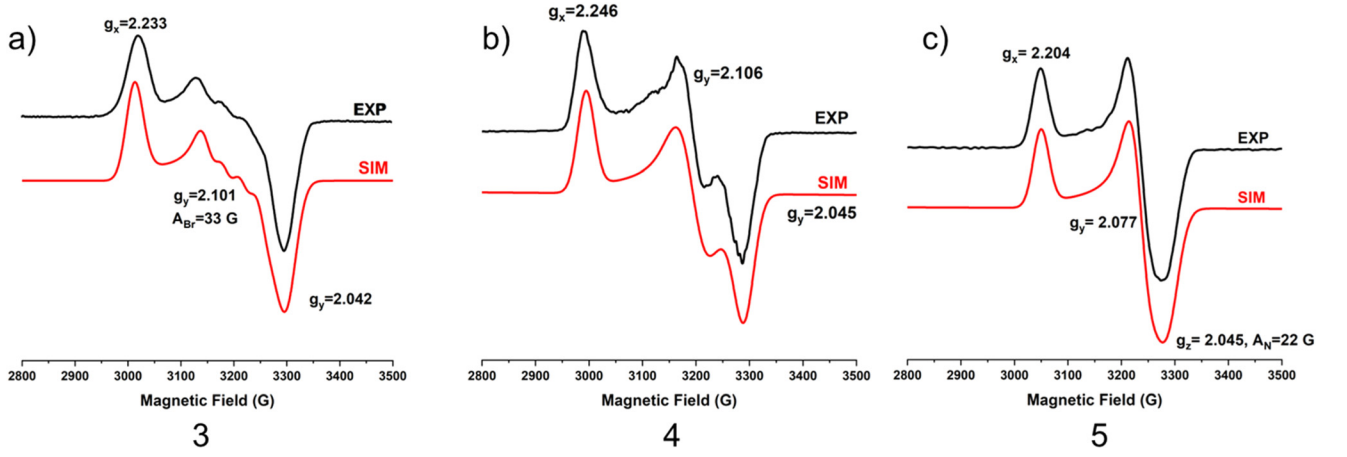

Fig. 2 The experimental and simulated EPR spectra of **3**, **4**, and **5** in PrCN at 77 K. Simulations were obtained using the following parameters: **1**: g_x = 2.233; g_y = 2.101 (A_{Br} = 33 G); g_z = 2.042; **2**: g_x = 2.246; g_y = 2.106; g_z = 2.045; **3**: g_x = 2.204; g_y = 2.077; g_z = 2.025 (A_{2N} = 22 G).

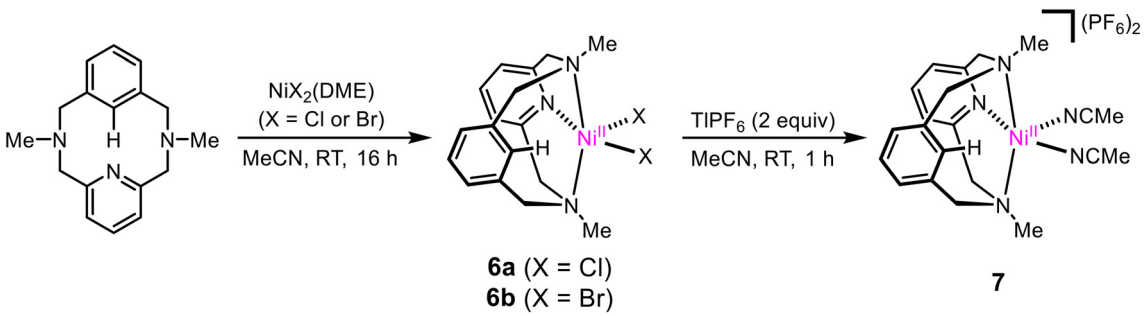

Scheme 2 Synthesis of $(^{Me}N3CH)Ni$ complexes.

this combination of hybrid functional and basis set has been previously demonstrated to accurately reproduce experimental parameters for Ni complexes.[42–44] The def2-TZVPP basis set was specifically employed to enhance a high level of accuracy in describing electron correlation effects, particularly the non-bonding interactions between the C–H bond and the metal center.[45–48] DFT calculations of the gas-phase structure of **6b** confirmed the non-bonding interactions of the C–H bond with the metal frontier orbitals (Fig. 3). Natural bond orbital (NBO) analysis of the HOMO further confirmed a weaker overlap between the σ (C–H)-bond and the d_{z^2}-orbital of nickel with a weak second order perturbation energy (E_2 = 2.3 kcal mol^{-1}). In a reverse fashion, the LUMO analysis shows the interaction of the metal orbital with the antibonding σ(C–H) bond, with an energy of 3.1 kcal mol^{-1} (Table S4†). We posit that these non-bonding interactions weaken the C–H bond and confirm the agostic interaction observed in this system.

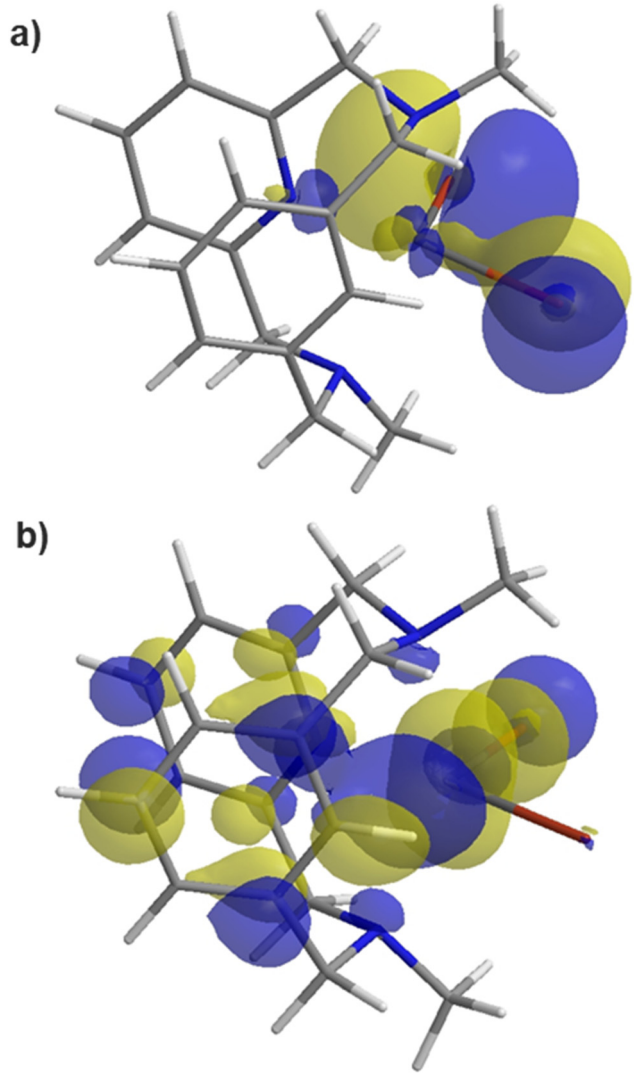

Fig. 3 Frontier beta molecular orbitals of **6b** (a) HOMO and (b) LUMO, shown as 0.03 isodensity surfaces, obtained by DFT (B3LYP/def2-TZVPP); the LUMO shows the interaction of C–H bonds with the Ni d orbital.

Ligand effect on properties of (^{R}N3CX)Ni complexes

Characterization of this series of complexes has allowed us to incorporate the (^{Me}N3CX)Ni series into the metrical and electrochemical trends observed in the (^{R}N3C)Ni systems bearing Np, ^{t}Bu, and H N-substituents.[28,29,49] It was previously noted that moving from the ^{tBu}N3C^{-} system to the less sterically hindered ^{Np}N3C^{-} system led to an increase in the axial amine donation, as evidenced by a decrease in the average axial Ni–N bond length (2.302 Å *vs.* 2.239 Å), and an increase in the superhyperfine coupling observed in the g_z direction (10 G *vs.* 14 G). Gratifyingly, the use of the ^{Me}N3C^{-} ligand corroborates this finding, bearing a significantly shorter average Ni–N bond distance of 2.147 Å, and a stronger superhyperfine coupling of 22 G with the axial N donors in the g_z direction. Finally, the reduction potential for the Ni$^{III/II}$ couple for the ^{Me}N3C^{-} system has been lowered by about 100 mV compared to the ^{Np}N3C^{-} system. With the ^{tBu}N3C^{-} system possessing a less-reeducing Ni$^{III/II}$ redox couple by an additional 150–300 mV, we see a continued trend of decreasing steric bulk on the axial N donors leading to lower reduction potentials. However, unlike the other two systems, ^{Me}N3C^{-} complexes exhibit irreversibility with the Ni$^{III/II}$ couple, though **3** demonstrates some quasi-reversibility at higher scan rates (see Fig. S8†). This trend also extends to the (^{R}N3CH)Ni complexes, though it is less pronounced. The (^{R}N3CH)NiBr$_2$ complexes for the N-^{t}Bu, N-Np, and N-Me derivatives exhibit average axial Ni–N bond distances of 2.608 Å, 2.309 Å, and 2.239 Å, respectively, demonstrating a clear decrease (Fig. 1). Similarly, when comparing the Ni-bisolvento complexes, the axial N donor atoms move much closer for H (2.158 Å) compared to Me (2.239 Å). However, for comparing Ni–C distances, the trend becomes much less clear. The Np and Me dibromide analogues possess approximately the same Ni–C bond distances at 2.479 Å and 2.482 Å, within the reported error. For the bis-solvento complexes, on the other hand, the Me complex bears a shorter Ni–C distance than the H complex, at 2.416 Å *vs.* 2.453 Å. This suggests that the ^{Me}N3CH complexes may exhibit stronger agostic interactions than the other ^{R}N3CH analogues and may also bear a stronger stabilization in the organometallic Ni complex, *via* donation from the axial N donors. Together, these observations indicate that ^{Me}N3CH may be best poised to undergo C–H activation reactivity.

Catalytic trifluoroethoxylation reactivity

To investigate the catalytic properties of these complexes, we initially examined complexes **2**, **5**, and **6b** in the trifluoroalkoxylation reaction with trifluoroethanol (Scheme 3). The Ribas group has recently reported the trifluoro- and difluoroethoxylation of Ni^{II} complexes supported by the ^{H}N3CH ligand.[49] Building on their findings, we sought to assess the steric effects of Ni complexes with the ^{Me}N3CH ligand by evaluating the reaction time and yield. The ethoxylation reaction was carried out under air in the presence of trifluoroethanol, $FcPF_6$

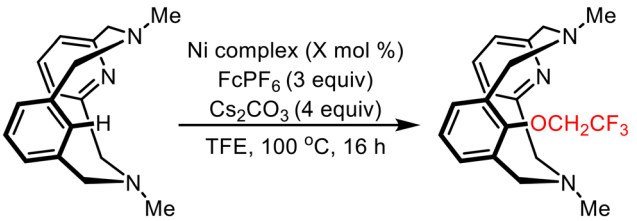

Scheme 3 General scheme for reactivity of 2,2,2-trifluoroethanol with Ni complexes.

as the oxidant, and Cs_2CO_3 as the base (Table 1). Among the complexes tested, **7** demonstrates catalytic conversion to the ethoxylated product in 49% yield and with a turnover number (~2) to that reported by the Ribas group. Only stoichiometric amounts of the product were obtained when **2** or **6b** was used as the catalyst, suggesting that regeneration of the active catalyst during the catalytic cycle was impeded. The reaction proceeds with similar yields when employing the nickel precursors for **6b** and **7**, rather than the pre-formed complexes (Table S1†). In contrast, a super-stoichiometric amount of C–O product was obtained for **5**, indicating that ethoxylation from a formally Ni^{III} center may be more operative compared to a Ni^{II} center as in **2**.

Stoichiometric C–C bond formation reactivity

We then investigated C–C bond formation using the Ni complexes in various oxidation states. The ^{Me}N3CH system supports Ni complexes in different oxidation states, and higher oxidation states of Ni are considered more effective in suppressing β-hydride elimination (βHE) – a common side reaction in C–C cross-coupling employing alkyl substrates. We performed stoichiometric C–C bond formation reactions using the complexes **1** and **3** with an octyl Grignard reagent (Scheme 4). The reaction likely leads to the *in situ* formation of Ni-alkyl complexes, creating a favorable environment for C–C coupling or βHE at the Ni center. Acidic workup of the reaction mixture results in the release of C–C coupled products, the β-hydride eliminated product octene, the protodemetalated product octane, and thus allowing us to measure the ratio of C–C coupling to βHE. The Ni^{II} complex **1** yields 9% of the C–C coupled product, while octene was produced in 37% yield (Table 2). In contrast, the Ni^{III} analog, complex **3**, more effectively suppresses βHE and produces a greater yield of the C–C coupled product than **1**. Specifically, the yield of ^{Me}N3C-octyl was 33%, while octene was produced in 21% yield. Additionally, the homocoupled hexadecane product was observed at a 3% yield with **3**, while none was observed for the Ni^{II} complex **1**. The outcome is likely a result of a monocationic Ni^{II} center being unable to bear an additional two anionic ligands, which is supported by a reaction using dicationic **7** (see Table S3†), which yields only 1% of the ^{Me}N3C-octyl coupled product but 9% hexadecane. The ratio of C–C coupling to βHE for the Ni^{II} complex was 0.24, whereas the Ni^{III} complex showed a much higher ratio of 1.7. Overall, the Ni^{III} complex more efficiently suppressed βHE and yielded the C–C coupled product at a higher efficiency compared to its Ni^{II} analogue. Interestingly, complex **3** reports a higher yield of both the ^{Me}N3C-octyl and hexadecane coupled products compared to the dichloride derivative **4**, even though one might expect more facile transmetallation with two chloride ligands. In this case, the loosely bound acetonitrile ligand may play a role in facilitating transmetallation and reductive elimination, as has been observed recently.[5]

Table 1 Catalytic trifluoroethoxylation of ^{Me}N3CH by Ni complexes

Entry	Complex	mol %	Yield (%)	Conversion (%)
1	**2**	30	24	38
2	**5**	30	33	45
3	**6b**	30	25	31
4	**7**	30	49	>99

Conclusion

In summary, herein we report the synthesis and characterization of a series of Ni^{II} and Ni^{III} complexes bearing the

Table 2 C–C bond coupling reaction of Ni^{II} (**1**) and Ni^{III} (**3**) complexes with octyl Grignard reagent (ND = not detected)

Complex	A	C	E	A : E	(A + C) : E
1	9 ± 2	ND	37 ± 2	0.24 ± 0.06	0.24 ± 0.06
3	33 ± 6	3 ± 1	21 ± 7	1.6 ± 0.6	1.7 ± 0.6

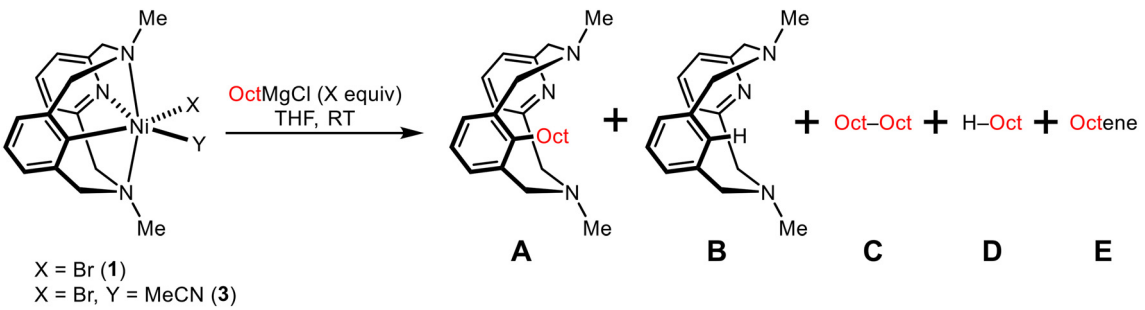

Scheme 4 General scheme for reductive elimination from Ni complexes and products formed.

^{Me}N3C^{-} or ^{Me}N3CH pyridinophane ligand framework. Analysis of the solid-state structures demonstrates the effect of the axial substituent on metrical parameters, particularly the proximity of the Ni center to the C_{sp^2}–H bond to support an agostic interaction. Catalytic ethoxylation of the ligand is observed using 2,2,2-trifluoroethanol, demonstrating its competence for C–O bond formation compared to the previously reported ^{H}N3CH variant. Reductive elimination studies from activated Ni^{II} and Ni^{III} centers shows the relevance for Ni^{III} in suppressing βHE from alkyl coupling partners in favor of productive cross-coupling routes. Overall, this study sheds light on organometallic Ni catalyst design from the ligand and metal perspective for future development of Ni C–H bond catalysts.

Data availability

Data for this article containing synthetic details, spectroscopic characterization, reactivity studies and computational details have been included as part of the ESI.† Crystallographic data for the structures reported in this article have been deposited at the Cambridge Crystallographic Data Centre, under CCDC 2390120 and 2390122–2390125.†

Conflicts of interest

The authors declare no competing financial interest.

Acknowledgements

We thank the National Science Foundation (CHE 2155160 to L. M. M.) for support. The authors gratefully acknowledge Dr Toby Woods and Dr Danielle Grey of the George L. Clark X-Ray Laboratory for invaluable assistance in collection and interpretation of the crystallographic data. We would also like to thank the NMR laboratory and staff at the University of Illinois Urbana-Champaign for their assistance and expertise.

References

1 N. Heberer, C.-H. Hu and L. M. Mirica, in *Comprehensive Coordination Chemistry III*, ed. E. C. Constable, G. Parkin and L. Que Jr, Elsevier, Oxford, 2021, pp. 348–374.
2 P. Mondal, P. Pirovano, A. Das, E. R. Farquhar and A. R. McDonald, *J. Am. Chem. Soc.*, 2018, **140**, 1834–1841.
3 J. S. Zhang, Y. M. Lee, M. S. Seo, M. Nilajakar, S. Fukuzumi and W. Nam, *Inorg. Chem.*, 2022, **61**, 19735–19747.
4 S. K. Kariofillis and A. G. Doyle, *Acc. Chem. Res.*, 2021, **54**, 988–1000.
5 L. Griego, J. B. Chae and L. M. Mirica, *Chem*, 2024, **10**, 867–881.
6 M. Carnes, D. Buccella, J. Y. C. Chen, A. P. Ramirez, N. J. Turro, C. Nuckolls and M. Steigerwald, *Angew. Chem., Int. Ed.*, 2009, **48**, 290–294.
7 P. J. Alonso, A. B. Arauzo, M. A. García-Monforte, A. Martín, B. Menjón, C. Rillo and M. Tomás, *Chem. – Eur. J.*, 2009, **15**, 11020–11030.
8 J. B. Diccianni, C. H. Hu and T. N. Diao, *Angew. Chem., Int. Ed.*, 2017, **56**, 3635–3639.
9 N. X. Gu, P. H. Oyala and J. C. Peters, *J. Am. Chem. Soc.*, 2020, **142**, 7827–7835.
10 H. Lee, J. Borgel and T. Ritter, *Angew. Chem., Int. Ed.*, 2017, **56**, 6966–6969.
11 E. Chong, J. W. Kampf, A. Ariafard, A. J. Canty and M. S. Sanford, *J. Am. Chem. Soc.*, 2017, **139**, 6058–6061.
12 C. C. Roberts, E. Chong, J. W. Kampf, A. J. Canty, A. Ariafard and M. S. Sanford, *J. Am. Chem. Soc.*, 2019, **141**, 19513–19520.
13 J. R. Bour, D. M. Ferguson, E. J. McClain, J. W. Kampf and M. S. Sanford, *J. Am. Chem. Soc.*, 2019, **141**, 8914–8920.
14 M. W. Milbauer, J. W. Kampf and M. S. Sanford, *J. Am. Chem. Soc.*, 2022, **144**, 21030–21034.
15 P. Roy, J. R. Bour, J. W. Kampf and M. S. Sanford, *J. Am. Chem. Soc.*, 2019, **141**, 17382–17387.
16 E. A. Meucci, A. Ariafard, A. J. Canty, J. W. Kampf and M. S. Sanford, *J. Am. Chem. Soc.*, 2019, **141**, 13261–13267.
17 E. A. Meucci, S. N. Nguyen, N. M. Camasso, E. Chong, A. Ariafard, A. J. Canty and M. S. Sanford, *J. Am. Chem. Soc.*, 2019, **141**, 12872–12879.
18 C. C. Roberts, N. M. Camasso, E. G. Bowes and M. S. Sanford, *Angew. Chem., Int. Ed.*, 2019, **58**, 9104–9108.
19 N. M. Camasso, A. J. Canty, A. Ariafard and M. S. Sanford, *Organometallics*, 2017, **36**, 4382–4393.
20 E. A. Meucci, N. M. Camasso and M. S. Sanford, *Organometallics*, 2017, **36**, 247–250.
21 X. Hu, *Chem. Sci.*, 2011, **2**, 1867–1886.
22 G. D. Jones, C. McFarland, T. J. Anderson and D. A. Vicic, *Chem. Commun.*, 2005, 4211–4213.
23 O. Vechorkin and X. Hu, *Angew. Chem., Int. Ed.*, 2009, **48**, 2937–2940.
24 R. Shi, Z. Zhang and X. Hu, *Acc. Chem. Res.*, 2019, **52**, 1471–1483.
25 H. Yin and G. C. Fu, *J. Am. Chem. Soc.*, 2019, **141**, 15433–15440.
26 W. Zhou, J. W. Schultz, N. P. Rath and L. M. Mirica, *J. Am. Chem. Soc.*, 2015, **137**, 7604–7607.
27 W. Zhou, N. P. Rath and L. M. Mirica, *Dalton Trans.*, 2016, **45**, 8693–8695.
28 W. Zhou, S. A. Zheng, J. W. Schultz, N. P. Rath and L. M. Mirica, *J. Am. Chem. Soc.*, 2016, **138**, 5777–5780.
29 W. Zhou, M. B. Watson, S. Zheng, N. P. Rath and L. M. Mirica, *Dalton Trans.*, 2016, **137**, 15886–15893.
30 A. J. Wessel, J. W. Schultz, F. Tang, H. Duan and L. M. Mirica, *Org. Biomol. Chem.*, 2017, **15**, 9923–9931.
31 S. I. Ting, W. L. Williams and A. G. Doyle, *J. Am. Chem. Soc.*, 2022, **144**, 5575–5582.
32 N. P. Ruhs, J. Khusnutdinova, N. P. Rath and L. M. Mirica, *Organometallics*, 2019, **38**, 3834–3843.

33 C. Magallón, O. Planas, S. Roldán-Gómez, J. M. Luis, A. Company and X. Ribas, *Organometallics*, 2021, **40**, 1195–1200.
34 O. Planas, C. J. Whiteoak, V. Martin-Diaconescu, I. Gamba, J. M. Luis, T. Parella, A. Company and X. Ribas, *J. Am. Chem. Soc.*, 2016, **138**, 14388–14397.
35 O. Planas, S. Roldán-Gómez, V. Martin-Diaconescu, T. Parella, J. M. Luis, A. Company and X. Ribas, *J. Am. Chem. Soc.*, 2017, **139**, 14649–14655.
36 O. Planas, S. Roldan-Gomez, V. Martin-Diaconescu, J. M. Luis, A. Company and X. Ribas, *Chem. Sci.*, 2018, **9**, 5736–5746.
37 L. Capdevila, M. Montilla, O. Planas, A. Brotons, P. Salvador, V. Martin-Diaconescu, T. Parella, J. M. Luis and X. Ribas, *Inorg. Chem.*, 2022, **61**, 14075–14085.
38 H. M. Dinh, Y. T. He, R. R. Fayzullin, S. Vasylevskyi, E. Khaskin and J. R. Khusnutdinova, *Eur. J. Inorg. Chem.*, 2023, **26**, e202300460.
39 A. Sarbajna, Y. T. He, M. H. Dinh, O. Gladkovskaya, S. M. W. Rahaman, A. Karimata, E. Khaskin, S. Lapointe, R. R. Fayzullin and J. R. Khusnutdinova, *Organometallics*, 2019, **38**, 4409–4419.
40 Y.-T. He, A. Karimata, O. Gladkovskaya, E. Khaskin, R. R. Fayzullin, A. Sarbajna and J. R. Khusnutdinova, *Organometallics*, 2021, **40**, 2320–2331.
41 M. Brookhart, M. L. H. Green and G. Parkin, *Proc. Natl. Acad. Sci. U. S. A.*, 2007, **104**, 6908–6914.
42 S. Chakrabarti, S. Sinha, G. N. Tran, H. Na and L. M. Mirica, *Nat. Commun.*, 2023, **14**, 905.
43 B. J. Shields, B. Kudisch, G. D. Scholes and A. G. Doyle, *J. Am. Chem. Soc.*, 2018, **140**, 3035–3039.
44 S. I. Ting, S. Garakyaraghi, C. M. Taliaferro, B. J. Shields, G. D. Scholes, F. N. Castellano and A. G. Doyle, *J. Am. Chem. Soc.*, 2020, **142**, 5800–5810.
45 E. Sutcliffe, D. A. Cagan and R. G. Hadt, *J. Am. Chem. Soc.*, 2024, **146**, 15506–15514.
46 K. J. Nelson, N. P. Kazmierczak, D. A. Cagan, A. H. Follmer, T. R. Scott, S. L. Raj, D. Garratt, N. Powers-Riggs, K. J. Gaffney, R. G. Hadt and A. A. Cordones, *J. Phys. Chem. Lett.*, 2024, **16**, 87–94.
47 D. A. Cagan, D. Bím, B. Silva, N. P. Kazmierczak, B. J. McNicholas and R. G. Hadt, *J. Am. Chem. Soc.*, 2022, **144**, 6516–6531.
48 Y. R. Poh, D. Morozov, N. P. Kazmierczak, R. G. Hadt, G. Groenhof and J. Yuen-Zhou, *J. Am. Chem. Soc.*, 2024, **146**, 15549–15561.
49 L. Capdevila, M. T. G. M. Derks, M. Montilla, J. M. Luis, J. Roithová and X. Ribas, *ChemistryEurope*, 2024, **2**, e202400023.

